

DIRECT CALIBRATION OF DISCRETE ELEMENT SIMULATION PARAMETERS FOR CORN PLANTER

/

玉米播种器离散元仿真参数的直接标定

Yang LI¹⁾, Yiteng LEI^{*1)}, Wei DONG¹⁾, Yulong CHEN²⁾

¹⁾ Intelligent Signal Capture and New Generation Communication Technology Laboratory, College of Electronic Engineering, Yili Normal University, Yining, Yili 835000, China;

²⁾ College of Agricultural Engineering and Food Science, Shandong University of Technology, Zibo 255000, China

Tel: +8615699398577; E-mail: younger1425580067@163.com

DOI: <https://doi.org/10.35633/inmateh-77-58>

Keywords: seed metering device, discrete element method, calibration, regression analysis

ABSTRACT

To improve the accuracy of contact parameters in discrete element simulations of seed metering devices and avoid errors arising during parameter measurement, this paper does not determine the values of each parameter in advance during parameter calibration. Instead, it directly uses the sliding friction angle, angle of repose, and rebound height as indicators, and employs regression analysis to calibrate the static friction coefficient, rolling friction coefficient, and restitution coefficient. The accuracy of the simulation parameters is verified through comparative experiments with the seed metering device. The results show that: the static friction coefficient is proportional to the sliding friction angle, and the correlation between the two is independent of material properties. The calibrated static friction coefficients between seeds, PMMA, and PLA are 0.39, 0.43, and 0.54, respectively; the rolling friction coefficient of seeds is exponentially related to the angle of repose, and the rolling friction coefficient between seeds is 0.029; the restitution coefficient is quadratically related to the rebound height in drop tests, and the calibrated restitution coefficients of seeds with PMMA and PLA are 0.33 and 0.32, respectively; the verification experiments demonstrate that the motion patterns of seed populations in simulation and physical experiments are similar, and the differences in seed filling rates between the two are not significant, proving the reliability of the calibrated simulation parameters.

摘要

为提高播种器离散元仿真接触参数的准确性, 避免参数测定过程中产生的误差, 本文在参数标定时不提前测定各参数的值, 直接以滑动摩擦角、休止角和反弹高度为指标, 利用回归分析方法, 对静摩擦系数、滚动摩擦系数和恢复系数进行标定, 并利用播种器的对比试验对仿真参数的准确性进行验证, 结果表明: 1) 静摩擦系数与滑动摩擦角成正比, 二者间的相关规律与材料性质无关, 标定得到种子与种子、PMMA、PLA 间的静摩擦系数分别为 0.39、0.43、0.54; 2) 种子的滚动摩擦系数与休止角成幂指数关系, 种子间的滚动摩擦系数为 0.029; 3) 恢复系数与跌落实验的反弹高度成二次函数关系, 标定后的种子与 PMMA 和 PLA 的恢复系数分别为 0.33、0.32; 4) 验证试验表明, 仿真试验与物理试验中种群的运动规律相似, 二者的充种率差异不显著, 证明标定后的仿真参数可靠。

INTRODUCTION

Corn is the cereal crop with the widest planting range and the largest production volume globally, ranking first among the three major food crops (corn, wheat, and rice) (Zhou et al., 2019). Corn can not only be consumed as food but is also widely used in feed, food processing, medical and healthcare, light industry, chemical industry, and bioenergy sectors (Xing et al., 2024). Therefore, the sustained high yield and high quality of corn are of great significance for food security and economic stability (Jia et al., 2022).

With the rapid development of modern agriculture, precision seeding using seed metering devices has become an important trend in agricultural mechanization (Hou et al., 2023). The working performance of the seed metering device directly determines the efficiency and precision of the entire seeding process, which is of great significance for improving the planting quality and yield of crops (Zhang et al., 2023).

¹⁾ Yang LI, lecturer; Yiteng LEI, Associate Professor; Wei DONG, assistant; Yulong CHEN, Associate Professor.

In recent years, in order to improve the operational performance of seeders, researchers at home and abroad have conducted extensive research on the seeding process and seed movement laws of seeders (Song *et al.*, 2025; Sharaby *et al.*, 2020). As a typical discrete material, seeds are widely studied using the discrete element method to investigate their motion patterns in seeders (Xu *et al.*, 2021; Zhang *et al.*, 2022; Mousaviraad *et al.*, 2024). The discrete element method is an effective numerical calculation method for analyzing the dynamics of dispersed particles by establishing a parameterized model of the solid particle system, simulating and analyzing particle behavior (Cundall *et al.*, 1988; Cundall *et al.*, 1979).

When conducting simulation experiments using the discrete element method, it is necessary to set the intrinsic parameters (particle Poisson's ratio, density, and shear modulus) and contact parameters (collision recovery coefficient, static friction coefficient, and sliding friction coefficient) of Figure 1 in the EDEM software (Chen *et al.*, 2023). The accuracy of simulation is directly related to the accuracy of simulation parameters. To enhance the accuracy of simulation, it is often necessary to calibrate the simulation parameters.

The calibration of simulation parameters primarily focuses on contact parameter. The conventional calibration method involves first conducting physical tests and calculating the values of contact parameters based on formulas. These values are then input into simulation software for virtual verification. By comparing virtual indicators with real indicators, appropriate adjustments are made to the parameters to obtain the final simulation parameters. However, due to the irregular structure of seed particles, significant variations in the parameters of different seeds, and differences in testing equipment and methods, there are considerable errors in parameter measurement (Wang *et al.*, 2015). Using parameters with errors for calibration increases the workload of calibration and makes it difficult to obtain accurate parameters. Moreover, there are often significant disparities in the parameters calibrated by different researchers (Zhang *et al.*, 2017).

MATERIALS AND METHODS

Seed

The corn variety MC607 (approval number: GSY 20176018), which is mainly cultivated in Xinjiang, China, was selected as the test subject. The test results showed that the 1000-grain weight was 351.4 g, the density was 1193kg/m³, and the moisture content was 11.8%.

Corn seeds can be divided into two major categories based on shape: flat and quasi-spherical. For ease of testing, this paper selects quasi-spherical seeds as the test subjects, with their dimensions expressed as length, width, and thickness (Figure 1). The length on the embryo surface along the direction from the radicle to the embryo is referred to as "length", the distance perpendicular to the "length" direction on the embryo surface is "width", and the distance from the embryo surface to the back is "thickness".

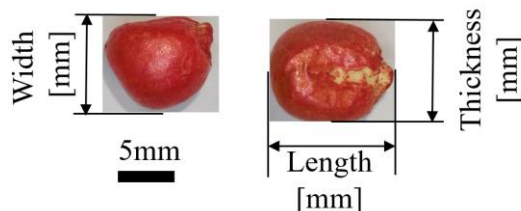


Fig. 1- Diagram of corn seed size

Select 100 quasi-spherical corn seeds and measure their three-axis dimensions. The average values of length, width, and thickness are 8.85 ± 0.35 mm, 8.29 ± 0.22 mm, and 7.59 ± 0.58 mm, respectively.

Through experiments and relevant literature, the Poisson's ratio of corn was found to be 0.44, and the shear modulus was 9.51×10^8 Pa (Wang *et al.*, 2018).

Contact materials

In the research process of seeding devices, transparent PMMA material is often used to process the shell of the seeding device in order to observe the movement patterns of seed populations. To accurately reflect the structural characteristics of the seeding disc and achieve rapid prototyping, 3D printing technology is widely used. PLA resin is a 3D printing material with excellent performance and low cost, so this paper mainly considers the contact parameters between seeds and PMMA and PLA.

Obtain the intrinsic parameters of PMMA and PLA through experiments and references (Zhang *et al.*, 2018) (Table 1).

Table 1

Intrinsic parameters of contact materials

Poisson's Ratio	Solid Density [kg·m ⁻³]	Shear Modulus [Pa]
PMMA	1218.9	8.2×10 ⁷
PLA	1454.7	1.2×10 ⁸

Simulation model

Conduct discrete element simulation experiments using Altair EDEM software (version 2022.0, Altair Engineering, Inc., USA), which is currently the mainstream discrete element software. Due to the lack of adhesion on the surface of corn seeds, the Hertz Mindlin non sliding model is chosen as the contact model in this article (Zhou *et al.*, 2014).

The discrete element simulation model of corn seeds is completed through automatic filling, consisting of eight spherical particles (Figure 2). The length, width, and thickness of the particles are set to 8.85, 8.29, and 7.59 mm, respectively, based on the measured values of the three-axis dimensions of the seeds.

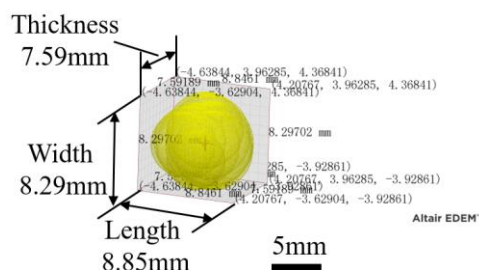
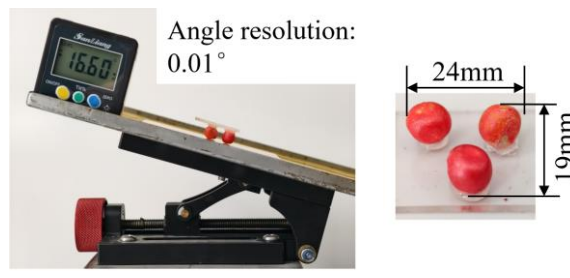


Fig. 2 - Discrete element simulation model of corn seed

Calibration method of static friction coefficient

During the parameter calibration experiment, a reasonable calibration experiment is designed based on the nature of the parameters. The experiment must be able to be conducted simultaneously in both virtual and real environments. The data obtained from testing in the real environment is used as the real indicator. The virtual indicator is compared with the real indicator. If the difference is not significant, the calibration is complete, and the simulation parameters at this time are the final parameters.

When calibrating the static friction coefficient between seeds and contact materials, the sliding friction angle is used as the calibration index (Zhang *et al.*, 2017). The material that rubs against the seeds is fixed on an inclined plane (Figure 3 (a)), which was made of high-precision aluminum alloy with a surface flatness tolerance of ± 0.05 mm, an effective working area of 300 mm \times 200 mm (length \times width), an angle adjustment mechanism with a measurement resolution of 0.01°, and a damping device on the rotation axis to achieve slow and uniform angle adjustment at a rate of < 0.5°/s for accurate capture of the initial sliding moment of seeds. The inclined plane is slowly rotated until the seeds start to slide, and the angle between the inclined plane and the horizontal plane at this moment is recorded as the sliding friction angle. To prevent seeds from rolling on the inclined plane, three seeds of similar size are glued together to form a seed plate (Figure 3 (b)), utilizing the stability of the triangle to ensure that each seed can be in close contact with the inclined plane.



a. Inclined plane meter b. Seed plate

Fig. 3- Measurement of static friction coefficient

When calibrating the static friction coefficient between seeds, the seed coat of corn was peeled off using a blade and placed flat on an inclined plane to measure the sliding friction angle between the seed and the seed coat.

During the simulation calibration process, to prevent the seed particles from rolling, each particle are modeled as a rectangular composite particle consisting of four spheres, with dimensions of 10 mm × 10 mm × 8 mm (length × width × thickness). In the simulation, a particle-generation factory (Fig. 4) with dimensions of 20 mm × 20 mm × 10 mm was established above the surface of the friction material. This configuration increases the contact area between the particle and the friction surface, thereby preventing rolling and aligning with the triangular stability observed in the physical seed plate. The number of generated particles was set to one, and each particle was placed flat on the friction-material surface.

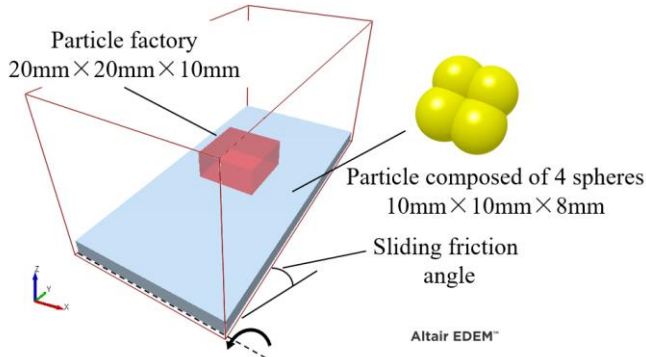


Fig. 4- Calibration method of static friction coefficient by simulation

Calibration method of rolling friction coefficient

When calibrating the rolling friction coefficient between seeds, use the angle of repose as the calibration indicator (Liu et al., 2016; Yang et al., 2016). The angle of repose is related to the static friction coefficient and rolling friction coefficient of particles, and the two friction coefficients are calibrated through reasonable experimental design. During the experiment, a cube box for holding corn seeds was made of transparent acrylic, with an internal dimension of 100 mm × 100 mm × 100 mm (length × width × height), a wall thickness of 5 mm to ensure structural stability and avoid interfering with seed accumulation observation, and one side designed as a removable baffle that could be vertically lifted at a constant speed of 0.05 m/s to ensure consistent seed spreading dynamics in each test. The seeds spread outward to form a slope, and the angle between the slope and the horizontal plane is the angle of repose.

Physical experiments were conducted (Figure 5(a)) and simulation experiments (Figure 5 (b)) separately.

To ensure accurate measurement of the angle of repose of corn seeds, images of the three-dimensional seed accumulation were first captured using a high-resolution camera. MATLAB software was then employed to process the images through a standardized workflow: 1) Noise reduction was performed using a Gaussian filter with a standard deviation (σ) of 1.5 to eliminate random image noise; 2) RGB images were converted to grayscale images using the formula $\text{Gray} = 0.2989\text{R} + 0.5870\text{G} + 0.1140\text{B}$ to simplify subsequent processing; 3) Adaptive binarization was implemented via the Otsu method to clearly segment the seed accumulation region from the background; 4) Edge detection was conducted using the Canny operator (with a low threshold of 50 and a high threshold of 150) to extract the contour of the seed accumulation; 5) A region of interest (ROI) was defined as the central 80% of the seed accumulation area to avoid edge interference caused by the test device. Finally, the least squares method was applied to fit the contour curve equation of one side of the seed accumulation, thereby realizing precise measurement of the angle of repose.

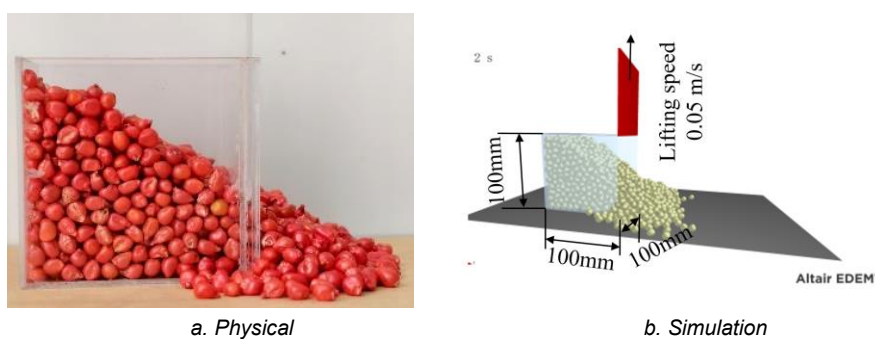


Fig. 5- Calibration principle of angle of repose

Calibration method of restitution coefficient

When calibrating the restitution coefficient e , the rebound height after the seed collides vertically with the contact material is used as the calibration indicator (Wang et al., 2012). The rebound height is measured using the free-fall collision method.

The instantaneous state of seed collision can be captured by a high-speed camera (Cui et al., 2013). In this paper, a Phantom V2512 high-speed camera with 3000 fps frame rate, 10 μ s exposure time and 50 mm fixed-focus lens was mounted 500 mm horizontally from the PMMA/PLA target surface (optical axis centered) to capture corn seed collision and rebound; a 2 m×1 m calibration board with 10 mm×10 mm grid was used for pre-test scale calibration, and two 500 W diffused LED fill lights (45° to target) provided uniform illumination to avoid seed surface shadows. The high-speed camera is used to record the rebound height after the seed comes into contact with the collision material, and the rebound height is recorded by reading the coordinates on a rear coordinate paper (Figure 6).



Fig. 6 - High speed camera calibration system of restitution coefficient

In the simulation calibration, a particle factory located 100 mm above the impact material in the discrete element software is set up (Figure 7). This factory generates only one particle, which falls freely with an initial velocity of 0 m/s.

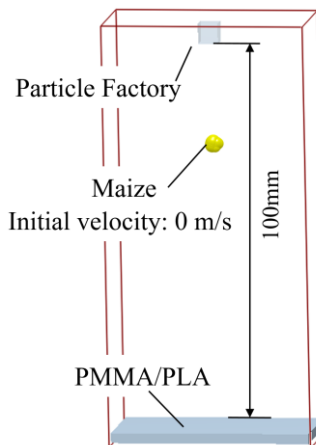


Fig. 7- Simulation calibration test of restitution coefficient

Seed metering performance verification test

A verification test for seed metering performance was conducted using a side-filling disc seed meter. The seed meter consists of a housing, a seed metering disc, a flange, a shaft, a base, and a sprocket component (Figure 8). During operation, as the seed metering disc passes through the seed group, seeds enter the seed pickup holes on the side of the disc, are adsorbed to the bottom of the holes by negative pressure, and are transported along with the holes to the seed dropping zone. When the negative pressure disappears, the seeds are dropped out.

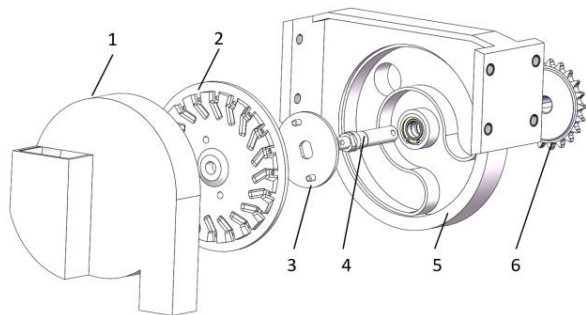


Fig. 8- Structure diagram of seed metering device
1-Shell; 2-Disk; 3-Flange; 4-Shaft; 5-Base; 6- Chain wheel

In the simulation software, the seed metering device was simplified by removing components such as the main shaft and flexible seed cleaning unit, retaining only the seed metering disc and shell. The seed metering disc was made of PLA material, while the shell was made of PMMA material.

During the experiment, the rotational speeds of the seed metering disc were set to 1.45 rad/s, 1.93 rad/s, 2.42 rad/s, and 2.91 rad/s, respectively, corresponding to forward speeds of the seeder of 6, 8, 10, and 12 km/h. In the simulation experiment, the number of particles generated by the particle factory was set to 400, and the simulation was conducted at the same rotational speeds as in the physical experiment.

Compare the motion patterns of populations during physical and simulation experiments. Because there is no negative pressure adsorption force applied in the simulation model, it is impossible to accurately reflect the situation of the seed planter taking a single seed. Therefore, the probability of the seed hole of the seed planter having a seed in it when it leaves the population is recorded as the filling rate.

$$F = \frac{h_1}{H} \times 100\% \quad (1)$$

where, F is the seed filling rate [%]; h_1 is the number of seed-taking holes with seeds, when leaving the population surface [-]; H is the total number of seed-taking holes. To ensure data reliability, all calibration tests including sliding friction angle for each contact combination, angle of repose and drop test for each material pair were repeated 5 times, abnormal data deviating from the mean by more than 2 standard deviations were excluded and results were expressed as mean \pm standard deviation.

RESULTS AND DISCUSSION

Calibration results of static friction coefficient

Simulation experiments were conducted with static friction coefficients of 0.10, 0.20, 0.30, ..., and 0.90, respectively, to obtain the simulation calibration results between particles and PMMA (Figure 9).

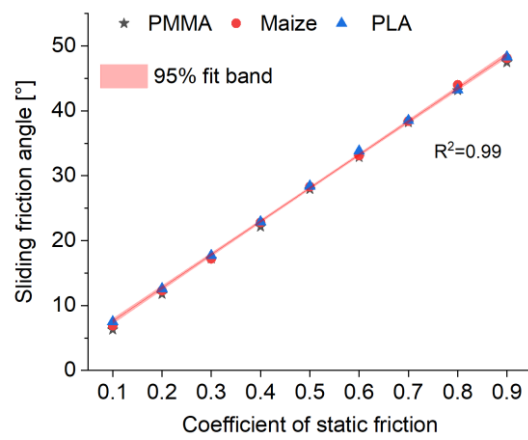


Fig. 9 - Test results of static friction coefficient calibration

Simulation results show that the correlation between the static friction coefficient and the sliding friction angle remains consistent for particles with different material properties, and the influence of the static friction coefficient on the sliding friction angle is independent of material properties. The static friction coefficient is linearly related to the sliding friction angle, and as the static friction coefficient increases, the sliding friction angle also increases.

Regression analysis was performed on the experimental data, and 95% confidence interval were calculated, resulting in the following regression equation between the static friction coefficient and the sliding friction angle:

$$y = 51.93x + 1.47, R^2 = 0.99 \quad (2)$$

where, y is the sliding friction angle [$^\circ$], x is the static friction coefficient [-], and R^2 is the coefficient of determination [-].

By substituting the measured sliding friction angles between seeds and corn, PMMA, PLA, which are $21.7^\circ \pm 0.2^\circ$, $23.8^\circ \pm 0.2^\circ$, and $29.5^\circ \pm 0.4^\circ$, respectively, into equation (2), the static friction coefficients were calculated as 0.39, 0.43, and 0.54, respectively.

Calibration results of rolling friction coefficient

The average angle of repose for corn, measured through physical prototype experiments, is $26.2^\circ \pm 0.3^\circ$.

To determine the relationship between the population angle of repose and the inter-particle restitution coefficient, the static friction coefficient was set to 0.39 and the rolling friction coefficient to 0.04. Simulation experiments were conducted in discrete element software with restitution coefficients of 0.2, 0.4, 0.6, and 0.8, respectively, to obtain the variation pattern of the population angle of repose (Figure 10). When the restitution coefficients were 0.2, 0.4, 0.6, and 0.8, the angles of repose were $25.5^\circ \pm 0.3^\circ$, $25.9^\circ \pm 0.4^\circ$, $26.1^\circ \pm 0.2^\circ$, and $25.6^\circ \pm 0.2^\circ$, respectively. The restitution coefficient had no significant effect on the angle of repose, which was only related to the static and rolling friction coefficients between seeds.

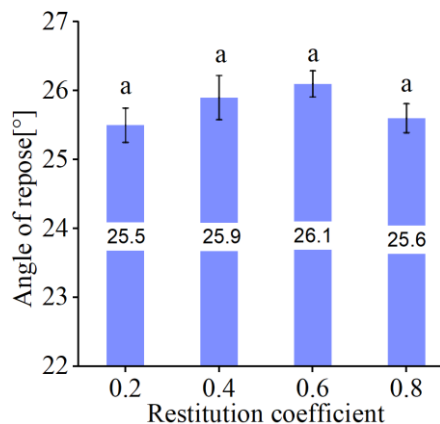


Fig. 10- The effect of restitution coefficient on angle of repose

Simulation calibration tests were performed in the discrete element software by setting the rolling friction coefficient to 0.01, 0.02, 0.03... 0.0. The influence of the rolling friction coefficient between seeds on the angle of repose was statistically analyzed (Figure 11). The rolling friction coefficient has a significant impact on the angle of repose, and as the rolling friction coefficient increases, the angle of repose gradually increases. When the rolling friction coefficient is 0.01, the angle of repose is $21.5^\circ \pm 0.1^\circ$. When the rolling friction coefficient increases to 0.05, the angle of repose is $29.8^\circ \pm 0.3^\circ$, an increase of 38.6%. When the rolling friction coefficient increases to 0.09, the angle of repose is $33.8^\circ \pm 0.4^\circ$, an increase of 13.4% compared to 0.05. As the rolling friction coefficient increases, the trend of increasing the angle of repose gradually slows down, and the angle of repose tends to stabilize.

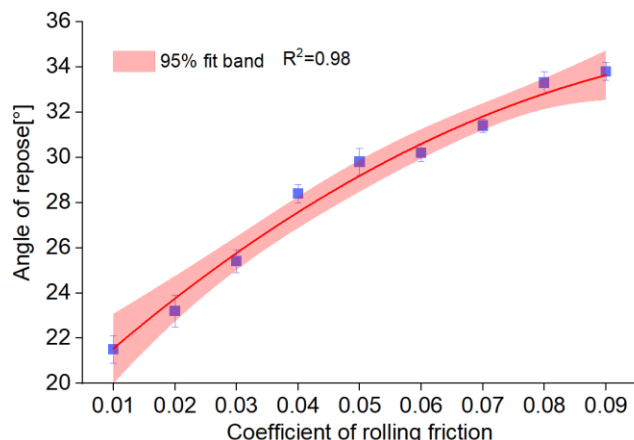


Fig. 11 - The effect of rolling friction coefficient on angle of repose

A regression analysis was conducted on the data, resulting in the relationship between the rolling friction coefficient and the angle of repose as follows:

$$y = 57.3x^{0.22}, R^2 = 0.98 \quad (3)$$

where, y is the angle of repose [°], x is the rolling friction coefficient, and R^2 is the coefficient of determination [-].

By substituting the measured value of the seed's angle of repose of $26.2^\circ \pm 0.3^\circ$ into equation (3), the rolling friction coefficient is obtained to be 0.029 ± 0.002 .

Calibration result of restitution coefficient

Place PMMA and PLA materials at the bottom of the drop frame, and release the seeds at zero speed from a set height of 100 mm. The measured collision rebound heights using a high-speed camera system are $18.3 \text{ mm} \pm 0.8 \text{ mm}$ and $16.2 \text{ mm} \pm 0.7 \text{ mm}$, respectively.

In EDEM, the restitution coefficients of the seeds and colliding materials were set to 0.1, 0.2, 0.3, ..., 0.9, respectively, and the rebound heights of the seeds after collision were measured (Figure 12).

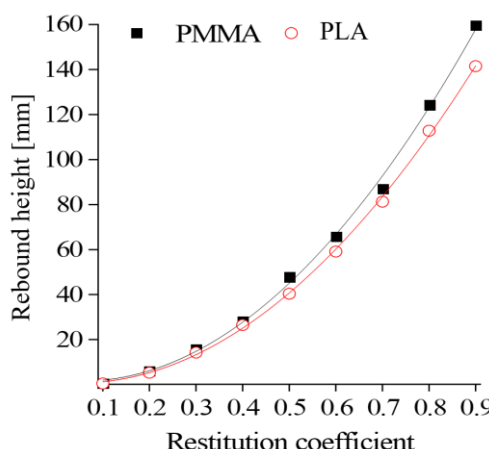


Fig. 12 - Calibration test results of restitution coefficient

The recovery coefficients of PMMA and PLA exhibit similar trends to the rebound heights. The recovery coefficient is directly proportional to the rebound height of the seed, and as the recovery coefficient increases, the rebound height also increases, with an increasingly stronger trend. Regression analysis of the experimental data yields the following regression equation between rebound height and recovery coefficient:

$$\begin{cases} y_1 = -23.1x_1^2 + 217.9x_1, R^2 = 0.99 \\ y_2 = -16.6x_2^2 + 192.1x_2, R^2 = 0.99 \end{cases} \quad (4)$$

In the formula, y_1 represents the rebound height of the seed after colliding with PMMA, y_2 represents the rebound height of the seed after colliding with PLA, x_1 represents the recovery coefficient between the seed and PMMA, and x_2 represents the recovery coefficient between the seed and PLA.

By substituting the measured values of the rebound height of collisions into equation (4), the restitution coefficients of the seed with PMMA and PLA were obtained as 0.33 and 0.32, respectively.

After conducting regression analysis and referencing literature (Li et al., 2013), the contact parameters of discrete element simulation were obtained (Table 2).

Table 2

Discrete element simulation contact parameters

	Restitution Coefficient	Static Friction Coefficient	Rolling Friction Coefficient
Seed-Seed	0.33	0.39	0.029
Seed-PMMA	0.32	0.43	0.032
Seed-PLA	0.32	0.54	0.038

Result of validation test

The rotational speeds of the physical prototype of the seed metering device were adjusted to 1.45 rad/s, 1.93 rad/s, 2.42 rad/s, and 2.91 rad/s for seed metering experiments. High-speed cameras were used to

observe the motion state of the seed population. In the pre-processing of EDEM, the rotational speed of the seed metering disc was set to be consistent with the physical experiment; the number of particles generated by the particle factory was set to 400 for simulation calculation, and the motion state of the seed population was observed (Figure 13).

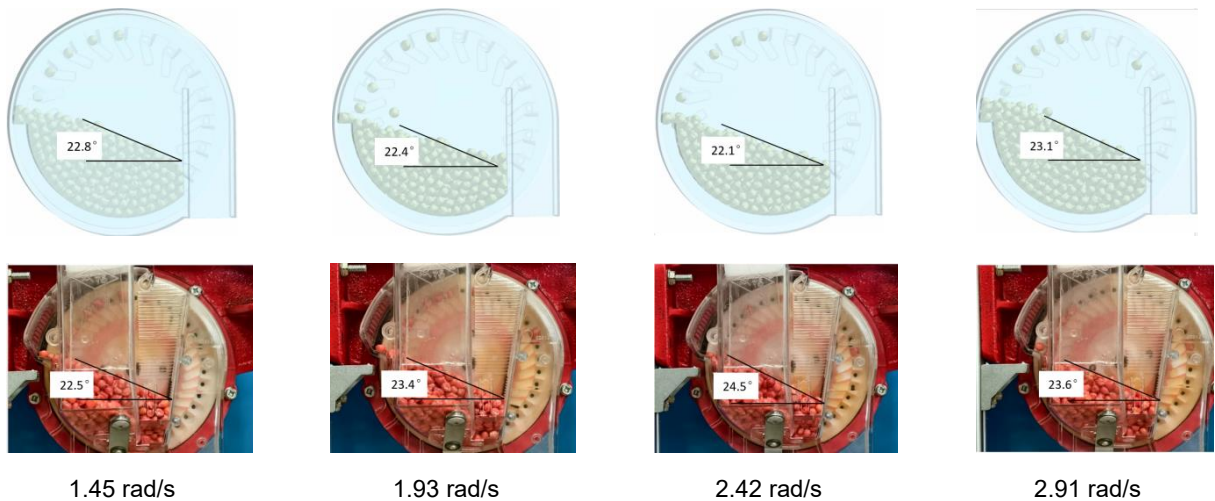


Fig. 13 - The movement of seeds

At different rotational speeds, the motion state of the seed population in the simulation experiment exhibits similar patterns to that observed in the physical experiment. As the rotational speed of the seed metering disc increases, the motion of the seed population becomes more intense. More and more seeds are lifted by the seed pickup holes and eventually fall back into the population. The range of the population fallback area gradually increases, and when the rotational speed reaches 2.91 rad/s, the range of the fallback area exceeds the middle position of the seed metering device.

The inclination angles of the population were measured in both physical experiments and simulation experiments. In the simulation experiment, when the rotational speed of the seed metering disc was 1.45 rad/s, the inclination angle of the population was 22.8°, and when the rotational speed was 2.91 rad/s, the inclination angle of the population was 23.1°. The influence of the rotational speed of the seed metering disc on the inclination angle of the population was not significant. In the physical experiment, the inclination angle of the population was similar to that in the simulation experiment, also maintaining around 23°.

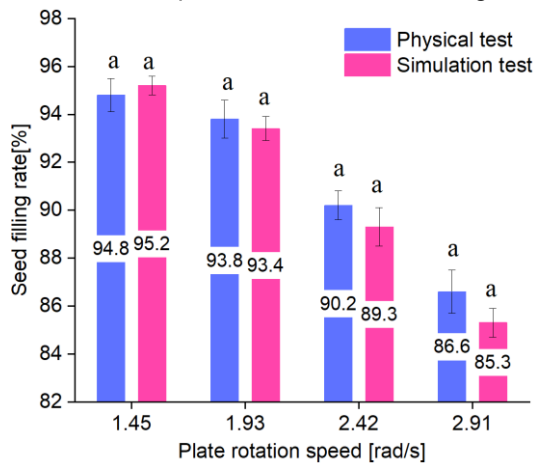


Fig. 14 - Results of validation tests

The seed filling rates in physical experiments and simulation tests were statistically analyzed separately (Figure 14). At a seed metering disc rotational speed of 1.45 rad/s, the seed filling rates in physical and simulation experiments were 94.8% and 95.2%, respectively. As the rotational speed increased, the seed filling rate significantly decreased. When the rotational speed reached 2.91 rad/s, the seed filling rates in physical and simulation experiments were 86.6% and 85.3%, respectively. At the same rotational speed, there was no significant difference in the seed filling rates between physical and simulation experiments, demonstrating the accuracy of the simulation parameters.

CONCLUSIONS

1) The static friction coefficient was calibrated using the sliding friction angle as the evaluation indicator, and the relationship between the static friction coefficient and the sliding friction angle was found to be consistent across all three materials. The static friction coefficient increases proportionally with the sliding friction angle. Based on regression analysis, the calibrated static friction coefficients for seeds against corn, PMMA, and PLA were determined to be 0.39, 0.43, and 0.54, respectively.

2) The angle of repose tests demonstrated that the coefficient of restitution had no significant influence on the measured angle of repose. Using the angle of repose as the calibration indicator, the rolling friction coefficient of corn seeds was determined. As the rolling friction coefficient increased, the angle of repose increased and eventually approached a stable value. Based on regression analysis, the calibrated rolling friction coefficient between seeds was determined to be 0.029.

3) The rebound height obtained from the drop tests was used as the indicator to calibrate the coefficient of restitution. The rebound height increased proportionally with the coefficient of restitution. Regression analysis yielded calibrated restitution coefficients of 0.33, 0.32, and 0.32 for seeds, PMMA, and PLA, respectively.

4) Verification experiments confirmed that the collective motion behavior in the simulation was consistent with that observed in the physical experiments. The intensity of particle motion increased with rotational speed, while the inclination angle of the seed mass remained stable at approximately 23°. The difference in seed filling rate between simulation and physical experiments was minimal, and the filling rate decreased notably as rotational speed increased. These results indicate that the calibrated simulation parameters have high accuracy.

ACKNOWLEDGEMENT

This work has received support from the Chinese Ministry of Education's Collaborative Education Project (202102257012).

REFERENCES

- [1] Boac, J. M., Casada, M. E., Pordesimo, L. O., Petingco, M. C., Maghirang, R. G., Harner, J. P. (2023). Evaluation of particle models of corn kernels for discrete element method simulation of shelled corn mass flow. *Smart Agricultural Technology*, Vol. 4, pp.100197. <https://doi.org/10.1016/j.atech.2023.100197>
- [2] Cundall, P. A. (1988). Formulation of a three-dimensional distinct element model—Part I. A scheme to detect and represent contacts in a system composed of many polyhedral blocks. *International Journal of Rock Mechanics and Mining Sciences & Geomechanics Abstracts*, Vol. 25, pp.107-116. [https://doi.org/10.1016/0148-9062\(88\)92293-0](https://doi.org/10.1016/0148-9062(88)92293-0)
- [3] Cundall, P. A., Strack, O. D. (1979). A discrete numerical model for granular assemblies. *Géotechnique*, Vol. 29, pp. 47-65. <https://doi.org/10.1680/geot.1979.29.1.47>
- [4] Cui, T., Liu, J., Yang, L., Zhang, D. X., Zhang, R., Lan, W. (2013). Experiment and simulation of rolling friction characteristic of corn seed based on high-speed photography (基于高速摄像的玉米种子滚动摩擦特性试验与仿真). *Transactions of the Chinese Society of Agricultural Engineering*, Vol. 29, pp.34-41.
- [5] Chen, Y., Gao, X. X., Jin, X. (2023). Calibration and Analysis of Seeding Parameters of *Cyperus Esculentus* Seeds Based on Discrete Element Simulation (油莎豆排种离散元仿真参数标定与试验). *Transactions of the Chinese Society for Agricultural Machinery*, pp.1-14.
- [6] Hou, Y. T. (2023). The Research Status and Development Trend of Precision Seeders (精量排种器的研究现状与发展趋势). *Modern Agricultural Equipment*, Vol. 44, pp.15-18.
- [7] Li, Z., Yu, J., Feng, Z., Fu, H., Zhang, L., Fei, X. (2013). Simulation and performance analysis of a soybean seed metering device using discrete element method. *Sensor Letters*, Vol.11, pp.1217-1222. <https://doi.org/10.1166/sl.2013.2897>
- [8] Liu, Y. Q., Zhao, M. Q. Liu, F., Yang, T. J., Zhang, T., Li, F.L. (2016). Simulation and optimization of working parameters of air-suction metering device based on discrete element (基于离散元的气吸式排种器工作参数仿真优化). *Transactions of the Chinese Society for Agricultural Machinery*, Vol. 47, pp.65-72. <https://doi.org/10.6041/j.issn.1000-1298.2016.07.010>

[9] Jia, S. L., Yu, J. Q., Ghayekhloo, T. (2022). Simulation Analysis and Construction of Maize Seeder Model Based on Edem (EM Solutions EDEM). *INMATEH Agricultural Engineering*, Vol. 63, pp.366-374. <https://doi.org/10.35633/inmateh-63-37>

[10] Mousaviraad, M., Tekeste, M. Z. (2024). Systematic Calibration and Validation Approach for Discrete Element Method (DEM) Modeling of Corn Under Varying Moisture Contents (MC). *Journal of the ASABE*, Vol. 67, pp.259-274. <https://doi.org/10.13031/ja.14763>

[11] Sharaby, N. N., Doroshenko, A. A., Butovchenko, A.V. (2020). Simulation of sesame seeds outflow in oscillating seed metering device using DEM. *Engineering Technologies and Systems*, Vol. 30, pp. 219-231. <https://doi.org/10.15507/2658-4123.030.202002.219-231>

[12] Song, S. D., Cai, X. H., Ye, Y., Dong, Z. G., Zhang, W. S., Li, G. L. (2025). Design and Experiment of Pneumatic Precision Seed Metering Device for Corn Plots (气吸式玉米小区精密排种器设计与试验). *Journal of Agricultural Mechanization Research*, pp.1-8. <https://doi.org/10.13427/j.issn.1003-188X.2025.12.015>

[13] Wang, C. J., Li, Y. M., Ma, L. Z., Ma, Z. (2012). Experimental study on measurement of restitution coefficient of wheat seeds in collision models (小麦籽粒碰撞模型中恢复系数的测定). *Transactions of the Chinese Society of Agricultural Engineering*, Vol. 28, pp.274-278.

[14] Wang, J. W., Tang, H., Wang, Q., Zhou, W. Q., Yang, W. P., Shen, H. G. (2015). Numerical simulation and experiment on seeding performance of pickup finger precision seed-metering device based on EDEM (基于 EDEM 软件的指夹式精量排种器排种性能数值模拟与试验). *Transactions of the Chinese Society of Agricultural Engineering*, Vol. 31, pp.43-50.

[15] Wang, M. M., Wang, W., Yang, L. Q., Zhang, K. F., Zhang, H. M. (2018). Calibration of discrete element model parameters for maize kernel based on response surface methodology (基于响应面法的玉米籽粒离散元参数标定). *Journal of South China Agricultural University*, Vol. 39, pp.111-117. <https://doi.org/10.7671/j.issn.1001-411X.2018.03.017>

[16] Xing, S. L., Zhao, W. Y., Qu, H. (2024). Current Situation Analysis and Development Trend of Maize Mechanized Harvesting Technology (玉米机械化收获技术现状分析及发展趋势). *Journal of Agricultural Mechanization Research*, Vol. 46, pp.9-14. <https://doi.org/10.13427/j.cnki.njyi.20240019.004>

[17] Xu, B., Zhang, Y. Q., Cui, Q. L., Ye, S. B., Zhao, F. (2021). Construction of a Discrete Element Model Of Buckwheat Grain and Calibration of Parameters. *INMATEH Agricultural Engineering*, Vol. 64, pp.175-184. <https://doi.org/10.35633/inmateh-64-17>

[18] Yang, Z. M., Guo, Y. M., Cui, Q. L., Li, H. B. (2016). Test and influence factors analysis of friction characteristics of millet (谷子摩擦特性试验及其影响因素分析). *Transactions of the Chinese Society of Agricultural Engineering*, Vol. 32, pp.258-264.

[19] Zhou, H. B., Chen, Y., Sadek, M. A. (2014). Modelling of soil-seed contact using the Discrete Element Method (DEM). *Biosystems Engineering*, Vol.121, pp.56 - 66. <https://doi.org/10.1016/j.biosystemseng.2014.02.006>

[20] Zhang, T., Liu, F., Zhao, M. Q., Liu, Y. Q. F., Li, L., Ma, Q., Zhang, Y., Zhou, P. (2017). Measurement of physical parameters of contact between soybean seed and seed metering device and discrete element simulation calibration. *Journal of China Agricultural University*, Vol. 22, pp.86-92. <https://doi.org/10.1007/s12206-025-0223-4>

[21] Zhang, T., Liu, F., Zhao, M., Fan, Q. Q., Yan, P. (2018). Determination of corn stalk contact parameters and calibration of discrete element method simulation (玉米秸秆接触物理参数测定与离散元仿真标定). *Journal of China Agricultural University*, Vol. 23, pp.120-127.

[22] Zhou, X. F., Wang, Y. X. (2019). Effects of exogenous jasmonic acid on photosynthetic characteristics of maize under salt stress (外源茉莉酸对盐胁迫下玉米光合特性的影响). *Journal of Jilin Normal University (Natural Science Edition)*, Vol. 40, pp.80-86. <https://doi.org/10.16862/j.cnki.issn1674-3873.2019.04.014>

[23] Zhang, P., Zhang, H., Li, J. M., Tan, C. L., Zhang, J. X. (2022). Parametric Calibration of Cotton Straw Parameters in Xinjiang Based on Discrete Elements. *INMATEH Agricultural Engineering*, Vol. 67, pp.314-322. <https://doi.org/10.35633/inmateh-67-32>

[24] Zhang, H. Q., Chen, Y. F., Qiao, P. (2023). Research Status and Development Trend of Corn Precision Seeding Machinery. *China Southern Agricultural Machinery*. Vol. 54, pp.166-168.